

Nanomechanics of carbon nanotubes

BY ANDRAS KIS^{1,*} AND ALEX ZETTL^{2,3,*}

¹*School of Engineering, Ecole Polytechnique Fédérale de Lausanne,
CH-1015 Lausanne, Switzerland*

²*Department of Physics, and Center of Integrated Nanomechanical Systems,
University of California at Berkeley, Berkeley, CA 94720, USA*

³*Materials Sciences Division, Lawrence Berkeley National Laboratory,
Berkeley, CA 94720, USA*

Some of the most important potential applications of carbon nanotubes are related to their mechanical properties. Stiff sp² bonds result in a Young's modulus close to that of diamond, while the relatively weak van der Waals interaction between the graphitic shells acts as a form of lubrication. Previous characterization of the mechanical properties of nanotubes includes a rich variety of experiments involving mechanical deformation of nanotubes using scanning probe microscopes. These results have led to promising prototypes of nanoelectromechanical devices such as high-performance nanomotors, switches and oscillators based on carbon nanotubes.

Keywords: nanotubes; nanomechanics; mechanical properties

1. Introduction to carbon nanotubes

Carbon nanotubes (CNTs) are the newest forms of carbon discovered in 1991 by Iijima (1991). Owing to their remarkable properties, this discovery has opened whole new fields of study in physics, chemistry and materials science. Nanotubes possess a unique combination of small size (diameters ranging from approx. 1 to 50 nm with lengths up to several mm; Zhu *et al.* 2002), low density—similar to that of graphite—high stiffness, high strength and a broad range of electronic properties from metallic to p- and n-doped semiconducting. The field of their potential applications is immense, including reinforcing elements in high-strength composites (Thostenson *et al.* 2001), electron sources in field emission displays (de Heer *et al.* 1995), small X-ray sources, ultra-sharp and resistant local probes (Dai *et al.* 1996), gas sensors (Collins *et al.* 2000) and components of future nanoscale electronics (Avouris 2002). In addition, they represent a widely used system for studying fundamental physical phenomena on the mesoscopic scale.

CNTs form two structurally distinct classes. The first to be discovered, multiwalled CNTs (MWNTs), exhibits a Russian doll-like structure of nested concentric tubes (figure 1*a,b*). The interlayer spacing can range from 0.342 to

* Authors for correspondence (andras.kis@epfl.ch; azettl@physics.berkeley.edu).

One contribution of 7 to a Theme Issue 'Nanotribology, nanomechanics and applications to nanotechnology II'.

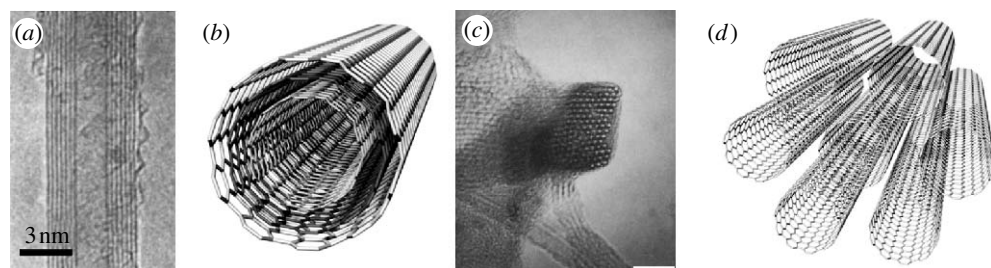


Figure 1. Two basic morphologies of CNTs with corresponding schematic. (a) Transmission electron microscope (TEM) image of a multiwalled carbon nanotube; adapted with permission from Iijima (1991). Copyright © Macmillan Publishers Ltd. (b) Schematic of a multiwalled nanotube. (c) TEM image of a bundle of single-walled CNTs. Scale bar, 10 nm; reprinted with permission from Thess *et al.* (1996). Copyright © AAAS. (d) A schematic of a bundle (rope) of single-walled nanotubes.

0.375 nm, depending on the diameter and number of shells comprising the tube (Kiang *et al.* 1998). The interlayer spacing in graphite is 0.335 nm, suggesting a similarly weak interaction between individual shells in MWNTs.

The second type of CNTs is in the basic form of a rolled-up graphitic sheet—a single-walled CNT (SWNT). During the production, their diameter distribution is relatively narrow, so they often bundle up in the form of crystalline ‘ropes’ (Thess *et al.* 1996; figure 1c,d) in which single tubes are held together by van der Waals interaction.

There are several ways of producing nanotubes. Small quantities of high-quality nanotubes can be produced by methods based on cooling carbon plasma that can be generated during an arc discharge between two graphitic electrodes in an inert atmosphere (Iijima 1991). Carbon plasma can also be formed by laser ablation of a graphitic target (Thess *et al.* 1996). Other methods, based on chemical vapour deposition (CVD) and catalytic decomposition of various hydrocarbons, e.g. methane or acetylene mixed with nitrogen or hydrogen in the presence of catalysts (Li *et al.* 1996), offer the possibility of controlling the growth of nanotubes by patterning the catalyst (Kong *et al.* 1998) and is therefore more suitable for producing nanoscale structures with integrated CNTs. This method is also capable of producing CNTs in industrial quantities. Their main disadvantage is the higher concentration of defects that diminish their stiffness (Salvetat *et al.* 1999a) and tensile strength (Barber *et al.* 2005; Kaplan-Ashiri *et al.* 2006).

2. Nanomechanics of CNTs

(a) Theoretical considerations

From the structural point of view, CNTs can be thought of as single sheets of graphite (graphene), rolled into a cylindrical shape with axial symmetry and diameters between 0.7 and 10 nm, typically approximately 1.2 nm. The ‘rolling-up’ of the graphene sheet (figure 2a) is described by the chiral vector that can

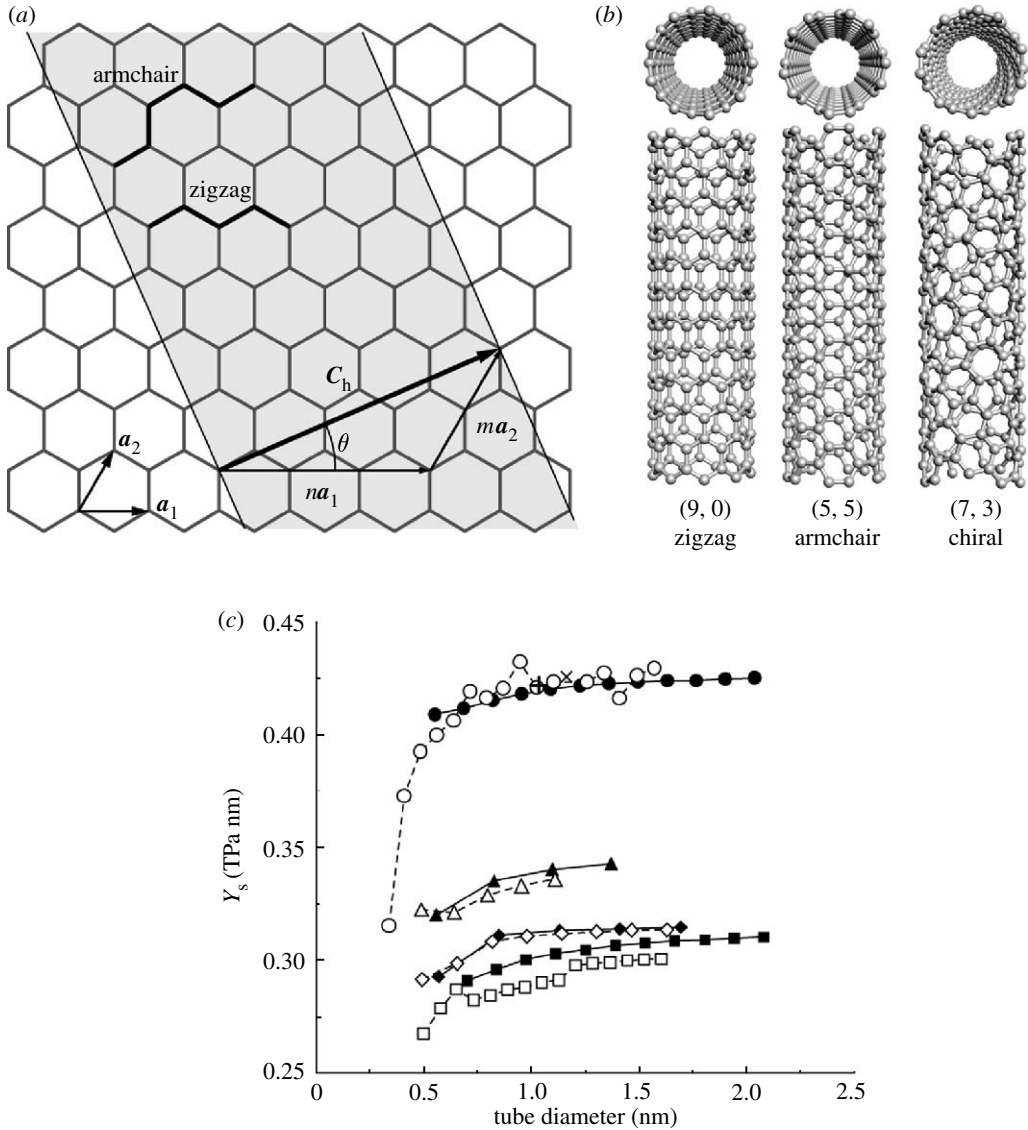


Figure 2. (a) Schematic of nanotube formation by ‘rolling-up’ a graphene sheet. (b) Models of zigzag, armchair and chiral nanotubes. (c) Young’s modulus as a function of diameter for C, BN, BC₃ and BC₂N nanotubes as calculated from tight-binding simulations (filled circles, C (n, n); open circles, C ($n, 0$); filled squares, BN (n, n); open squares, BN ($n, 0$); filled diamonds, BC₃ (n, n); open diamonds, BC₃ ($n, 0$); filled triangles, BC₂N (n, n); open triangles, BC₂N ($n, 0$); Hernández *et al.* 1998). Reprinted with permission from Hernández *et al.* (1998). Copyright © American Physical Society.

be expressed as

$$\mathbf{C}_h = n\mathbf{a}_1 + m\mathbf{a}_2 \equiv (n, m), \tag{2.1}$$

where integers n and m represent the chiral indices and $|\mathbf{a}_1| = |\mathbf{a}_2| = 2.49 \text{ \AA}$ is the lattice constant of graphite. Special cases are ‘zigzag’ ($n, 0$) and ‘armchair’ (n, n) nanotubes (figure 2b).

According to electronic properties, nanotubes can be semiconducting or metallic, depending on the chirality (Mintmire *et al.* 1992; Saito *et al.* 1992; Blase *et al.* 1994; Chico *et al.* 1996). CNTs are always produced with a distribution of chiralities and electrical properties over which there is no real control. From the mechanical point of view, strength and Poisson's ratio show the most pronounced chirality dependence, while Young's modulus is practically independent of chirality for nanotubes with diameters above 0.7 nm (Hernández *et al.* 1998).

Mechanical properties of CNTs are closely related to those of graphite. Stiff sp^2 -hybridized in-plane bonds (σ -bonds), 1.42 Å long, give them an exceptionally high Young's modulus while out-of-plane π -bonds, responsible for the main features of the electronic properties, govern the weak van der Waals interlayer cohesion. Different shells of MWNTs interact through the van der Waals interaction (in the absence of structural defects) while SWNTs form bundles in which the intertube coupling is also determined by the van der Waals interaction. The combination of strong sp^2 bonding and weak van der Waals interaction in these structures lies at the origin of the exceptionally diverse mechanical behaviour of nanotubes. Graphite is considered to be mechanically weak by the general public due to the fact that layers can be easily sheared apart, even though the in-plane stiffness of these layers is almost the same as the stiffness of diamond (Lu 1997). In analogy to graphite, the van der Waals interaction holding together SWNTs in bundles allows easy sliding between nanotubes and is responsible for the decreased resistance of these structures to bending.

In order to relate to mechanical properties, concepts like Young's modulus should be introduced at the nanoscale, which might seem puzzling at first. Electronic and thermal properties at this scale display behaviour in the realm of quantum physics, yet classical laws seem to be adequate for describing the mechanical properties. The reason for this is that Hooke's law can be applied to a series expansion of any potential around the equilibrium position. Young's modulus can thus be defined in terms of stress energy as

$$E_{\text{Young}} = \frac{1}{V_0} \left. \frac{\partial^2 E}{\partial \varepsilon^2} \right|_{\varepsilon=0}, \quad (2.2)$$

where V_0 is the equilibrium volume and E the strain energy. In the case of a single-walled nanotube, this requires adopting a convention for the effective thickness of graphene. Yakobson *et al.* first proposed the extent of π -orbitals, $t=0.066$ nm (Yakobson *et al.* 1996), resulting in spectacular values of roughly 5 TPa for Young's modulus of CNTs. Lu proposed another convention, the one that is in widespread use today, choosing the interlayer separation of graphite as the nanotube's thickness ($t=0.34$ nm). This gave a more reasonable value of 0.97 TPa for Young's modulus (Lu 1997), which is in good agreement with the C_{11} elastic constant of graphite (1.06 TPa in the basal plane; Blakslee *et al.* 1970; Seldin & Nezbeda 1970). Using an empirical potential, Lu also found that Young's modulus of nanotubes was practically independent of the tube's chirality and diameter (in the range 0.68–27 nm).

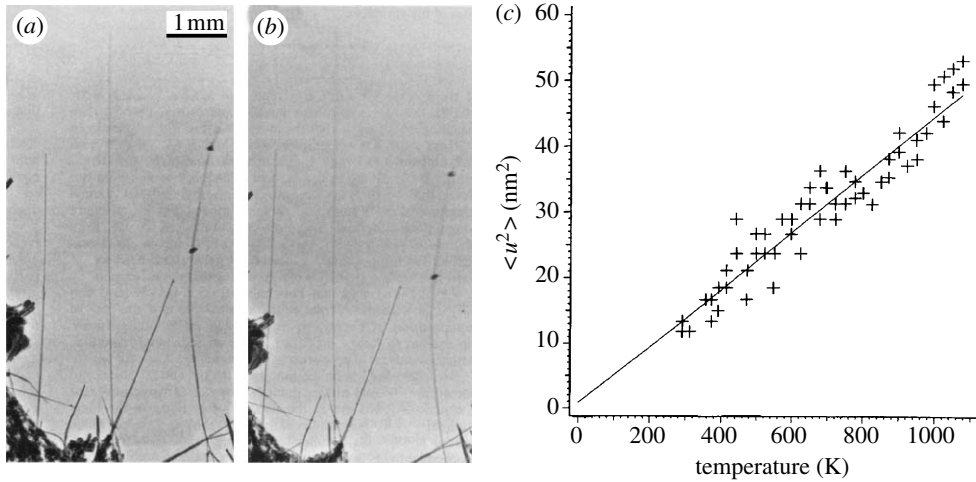


Figure 3. TEM images of a cantilevered MWNT showing blurring at the tips due to thermally excited vibration at the free end. Images were recorded at different temperatures: (a) 300 K and (b) 600 K. (c) Plot of the mean-square vibration amplitudes versus temperature for a 5.1 μm long and 16.6 nm thick nanotube. The effective E_{Young} was 3.7 ± 0.2 GPa (Treacy *et al.* 1996). Adapted with permission from Treacy *et al.* (1996). Copyright © Macmillan Publishers Ltd.

First calculations based on the tight binding by Hernández *et al.* (1998) resulted in a typical value of 1.22 TPa for Young's modulus of SWNTs, with a small dependence on the tube diameter (figure 2c) for tubes with diameters above 0.7 nm. Young's modulus decreases as the diameter is decreased due to rehybridization of bonds in highly curved tubes.

The mechanical response of CNTs to large deformations, including breaking and the associated morphological changes, was first studied by Yakobson *et al.* (1996) using molecular dynamics simulations. With properly chosen parameters, this analytical tool can predict nanotube behaviour not only at small deformations but also beyond the linear response.

(b) Mechanical measurements: bending and stretching

(i) Vibration inside a transmission electron microscope

First measurements of the mechanical properties of CNTs were based on measuring the amplitude of thermally induced vibration inside a transmission electron microscope (TEM) by Treacy *et al.* (1996). MWNTs were fixed at one end. The other end appeared blurred on TEM images due to thermal excitation (figure 3a,b).

The nanotube was modelled as a stochastically driven resonator and E_{Young} estimated from its Gaussian vibrational profile whose standard deviation σ is given by

$$\sigma^2 = \frac{16L^3 k_B T}{\pi E_{\text{Young}} (D^4 - D_{\text{int}}^4)} \sum_n \beta_n^{-4} \approx 0.4243 \frac{L^3 k_B T}{E_{\text{Young}} (D^4 - D_{\text{int}}^4)}, \quad (2.3)$$

where L is the cantilevered beam's length; k_B the Boltzmann constant; T the temperature; D and D_{int} the nanotube outer and inner diameters; and β_n a numerical constant for vibrational mode n .

From a series of measurements performed as a function of temperature (figure 3c), an average value of E_{Young} of 1.8 GPa was obtained. A variation of this method has also been applied to BN nanotubes (Chopra & Zettl 1998).

Another method based on exciting the mechanical resonance of nanotubes inside a TEM has been demonstrated by Poncharal *et al.* (1999). MWNTs were directly excited using an AC electric field and the E_{Young} was calculated from the frequencies of the first two resonant modes. Nanotubes were fixed on a specially designed TEM holder equipped with a piezo translation stage. Their motion is electrostatically induced by applying an AC voltage to the nanotubes that are at a distance of 5–20 μm from a grounded counterelectrode. The bending modulus E_{bending} can be calculated from the resonant frequency using a formula from the Bernoulli–Euler analysis of cantilevered elastic beams

$$\nu_j = \frac{\beta_j^2}{8\pi} \frac{1}{L^2} \sqrt{(D^2 + D_{\text{int}}^2)} \sqrt{\frac{E_{\text{bending}}}{\rho}}, \quad (2.4)$$

where D is the outer diameter; D_{int} the inner diameter; ρ the density; and β_j a constant for the j th harmonic: $\beta_1 = 1.875$ and $\beta_2 = 4.694$. For nanotube diameters below 10 nm, a typical value of 1 TPa was obtained for E_{bending} , while it dropped to 100 GPa for thicker tubes.

(ii) *Lateral bending induced by an atomic force microscope*

Set-ups in which the mechanical properties of nanotubes can be directly probed by applying a known force are usually based on atomic force microscopy (AFM). The first quantitative measurement of Young's modulus of MWNTs (and SiC nanorods) using an AFM-based set-up was reported by Wong *et al.* (1997). MWNTs were first randomly dispersed on a flat surface of MoS₂ single crystals, chosen owing to their low friction coefficient and flat surface. Friction between the tubes and substrate was further reduced by performing the measurements in water. Tubes were pinned on one side to this substrate by a deposition of an array of square pads through a shadow mask (figure 4a–c).

Nanotubes were deformed laterally by the AFM tip, until at a certain deformation the tip would pass over the tube, allowing the tube to snap back to its relaxed position. During measurements, lateral force–distance curves were acquired at different positions along the chosen beam (figure 4d,e).

The lateral force is known only up to a factor of proportionality because the AFM lever's lateral force constant was not calibrated for these measurements. This uncertainty and the effect of friction were eliminated by modelling the nanotube as a beam and calculating its lateral force constant:

$$\frac{dF}{dy} \equiv k = \frac{3\pi D^4}{64x^3} E_{\text{Young}}, \quad (2.5)$$

where E_{Young} is Young's modulus of the beam; D its diameter; and x the position along the beam. Corresponding experimental values are shown in figure 5. The mean value for Young's modulus of MWNTs was $E_{\text{Young}} = 1.3 \pm 0.6$ TPa,

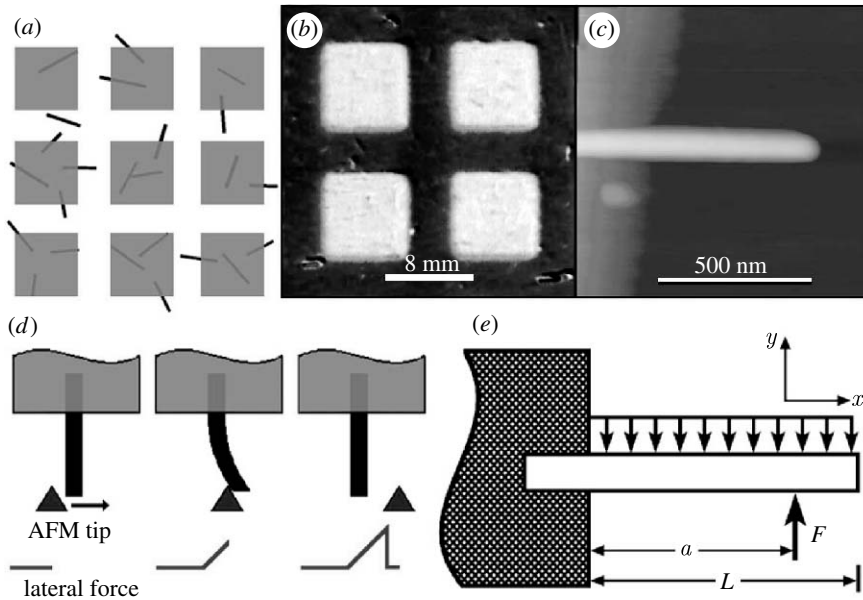


Figure 4. (a) Nanotubes are dispersed on a substrate and pinned down by SiO pads. (b) Optical micrograph of the sample. (c) AFM image of a SiC nanorod protruding from the pad. (d) The tip moves in the direction of the arrow. The lateral force is indicated at the bottom. During bending, the lateral force increases until the point at which the tip passes over the beam which snaps back to its initial position. (e) The beam of length L is subjected to a point load F at $x=a$ and friction force f (Wong *et al.* 1997). Reprinted with permission from Wong *et al.* (1997). Copyright © AAAS.

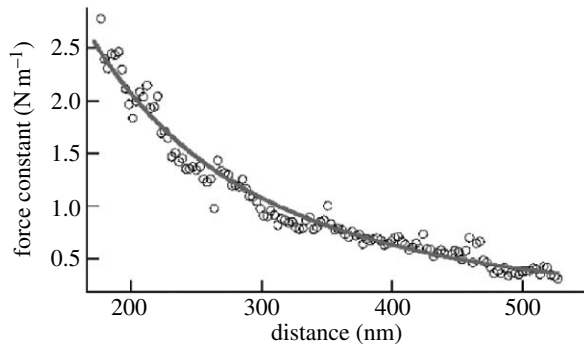


Figure 5. The lateral spring constant as a function of position on the beam. The curve is a fit to equation (2.5) (Wong *et al.* 1997). Reprinted with permission from Wong *et al.* (1997). Copyright © AAAS.

similar to that of diamond ($E_{\text{Young}} = 1.2 \text{ TPa}$). For larger deformations, discontinuities in bending curves were also observed, attributed to buckling of nanotubes.

Nanotubes with lengths that are much larger than their diameters are better described as elastic strings (rather than beams), with sp^2 bonds keeping the string under tension. Upon deformation, all of the strain goes into stretching the string.

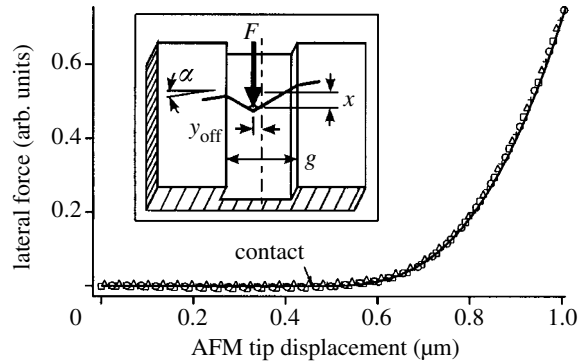


Figure 6. Lateral force on a single-walled nanotube rope as a function of AFM tip displacement (Walters *et al.* 1999). Reprinted with permission from Walters *et al.* (1999). Copyright © American Institute of Physics.

In the picture of beam bending, some portions of the same beam are compressed while others are stretched. This results in different dependence of force F on deformation x : for beam bending $F \sim x$ whereas for elastic strings $F \sim x^3$.

This point was shown in the experiments performed by Walters *et al.* who deformed suspended SWNT bundles in the lateral direction using an AFM (figure 6). The force F exerted on the tube by the AFM tip is given by the expression

$$F = 2T \sin \theta = 2T \frac{2x}{L} \approx \frac{8kx^3}{L_0}, \quad (2.6)$$

where T is the tension in the string; L_0 its equilibrium length; k the spring constant; and x the lateral deflection in the middle. Using this set-up, Walters *et al.* (1999) deformed SWNT ropes to the maximal strain of $5.8 \pm 0.9\%$ and determined a lower bound of 45 ± 7 GPa on the tensile strength, assuming a value of 1.2 TPa for Young's modulus.

(iii) Vertical bending induced by AFM

In a series of demanding experiments, Salvétat *et al.* measured Young's modulus of isolated SWNTs and SWNT ropes (Salvetat *et al.* 1999b), MWNTs produced using different methods (Salvetat *et al.* 1999a) and the shear modulus of SWNT ropes (Salvetat *et al.* 1999c). The experimental set-up that made measurements possible on such a wide range of CNT morphologies involved measuring the vertical deflection of nanotubes bridging holes in a porous membrane (figure 7a).

Nanotube samples for mechanical measurements are prepared by depositing CNTs on the surface of a flat alumina (Al_2O_3) ultrafiltration membrane. Some of the tubes end up suspended over holes in the filter, firmly held in place by the van der Waals interaction between the unsuspended parts of the tube and the membrane (figure 7a). A series of contact mode AFM images of the nanotube is taken under increasing mechanical load. Line scans across the tube (figure 7a) reveal the vertical deformation. In the case of SWNT bundles, a term describing sliding between tubes comprising the bundle has to be included in the formula for mechanical deformation. This easy sliding is due to the van der Waals

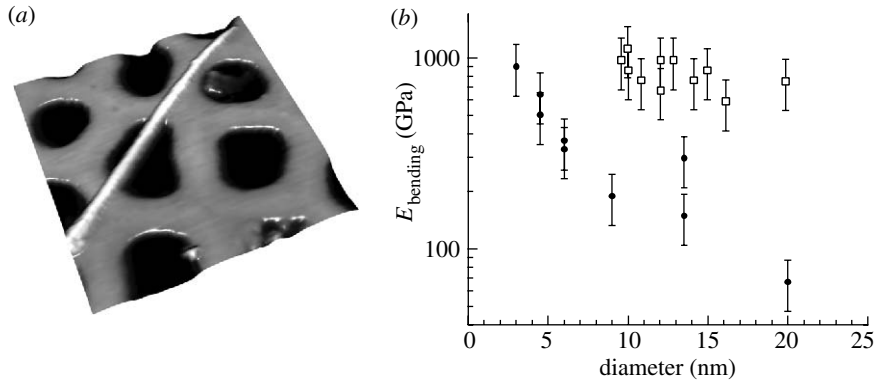


Figure 7. (a) Three-dimensional rendering based on an AFM image of a 10 nm thick SWNT bundle on a porous substrate used by Salvetat *et al.* for their mechanical measurements (Salvetat *et al.* 1999a). (b) Values of the bending modulus for 12 SWNT bundles (filled circles) of different diameters. The measured E_{bending} of thin bundles corresponds to E_{Young} , while for thick bundles one obtains the value of the shear modulus G (Salvetat *et al.* 1999c). MWNT (open squares) data are for arc-discharge grown tubes (Salvetat *et al.* 1999a).

interaction that holds the individual tubes together. Owing to this, bundles behave more as a loose assembly of individual tubes than as a compact beam. The deformation can thus be modelled as a sum of deflection due to bending and shear deformation (Gere & Timoshenko 1984):

$$\delta = \delta_{\text{bending}} + \delta_{\text{shearing}} = \frac{FL^3}{192E_{\text{Young}}I} + f_s \frac{FL}{4GA} = \frac{FL^3}{192E_{\text{bending}}I}, \quad (2.7)$$

where f_s is the geometric factor, equal to 10/9 for a cylinder; G the intertube shear modulus; and A the area of the beam's cross section. E_{bending} is the effective bending modulus, equal to Young's modulus in the case where the influence of intertube shearing can be neglected. This is the case with MWNTs.

Both the Young and the intertube shear moduli can be determined by measuring E_{bending} as a function of bundle diameter to length ratio and extrapolation. For thin ropes, bending modulus thus corresponds with Young's modulus, while for thick ropes one obtains the value of the intertube shear modulus G , of the order of 1 GPa.

This apparent structural weakening due to intertube shearing is a serious hindrance in using CNTs as building blocks in macroscopic structures as, for example, in ribbons, cables or composite materials (Vigolo *et al.* 2000). One way of solving this problem could be the creation of stable bonds between neighbouring tubes, for example, by electron beam irradiation (Kis *et al.* 2004).

Young's modulus is of the order of 1 TPa for both isolated SWNTs and MWNTs, which do not show any dependence of the mechanical response on the tube diameter (figure 7b). Different synthesis methods can result in widely varying Young's modulus of CNTs, due to degradation of the graphitic structure with the introduction of defects during production. An average value of $E_{\text{Young}}=870$ GPa was found for the arc-discharge grown tubes, while the

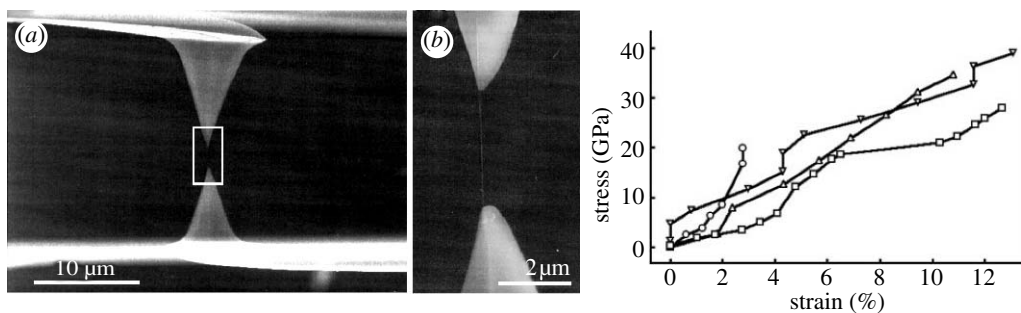


Figure 8. (a) An SEM image of a MWNT mounted between two opposing AFM tips. (b) A close-up of the region indicated by a rectangle in (a). (c) Plot of stress versus strain curves for different individual MWNTs (Yu *et al.* 2000a). Reprinted with permission from Yu *et al.* (2000a). Copyright © AAAS.

catalytically grown MWNTs, known to include a high concentration of defects, can have a Young's modulus as low as 12 GPa (Salvetat *et al.* 1999a; Lukić *et al.* 2005a), demonstrating the use of this measurement method in choosing the optimal synthesis conditions for producing CNTs with favourable mechanical properties (Lukić *et al.* 2005b).

(iv) Tensile loading

The first direct measurements of the elastic properties of CNTs that have not relied on the bending beam or stretching string set-up involved deforming MWNTs (Yu *et al.* 2000a) and SWNT ropes (Yu *et al.* 2000b) under axial strain. This was achieved by identifying and attaching opposite ends of MWNTs or SWNT ropes to two AFM tips, all inside a scanning electron microscope (SEM).

One tip was integrated with a rigid cantilever with a spring constant above 20 N m^{-1} and the other was compliant (0.1 N m^{-1} ; figure 8). The rigid lever was then driven using a linear piezomotor. On the other end, the compliant lever bent under the applied tensile load. The deflection of the compliant cantilever—corresponding to the force applied on the nanotube—and the strain of the nanotube were simultaneously measured.

From stress–strain curves obtained in this fashion (figure 8c), E_{Young} ranging from 270 to 950 GPa were found. Examination of broken tubes inside a TEM revealed that nanotubes break with the ‘sword-in-sheath’ mechanism, where only the outer layer appears to have carried the load. After failure, pull-out of inner shells follows. An average bending strength of 14 GPa and axial strengths up to 63 GPa were found. Firm attachment of nanotubes to AFM tips was ensured by a deposition of carbonaceous material induced by the electron beam concentrated in the contact area (Fujii *et al.* 1991).

(c) Mechanical measurements: interlayer force

In analogy with graphite, the van der Waals interaction between concentric shells of MWNTs could act as a form of lubrication and allow a host of potentially useful applications with MWNTs as building blocks of nanoelectromechanical

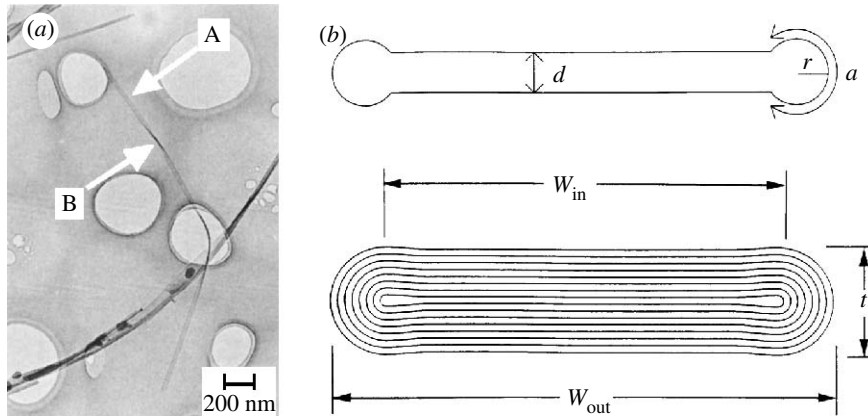


Figure 9. (a) TEM image of a collapsed nanotube; A and B point to flat regions of the ribbon, twisted with respect to each other. (b) Schematic collapsed single- and multiwalled tubes together with geometric parameters used to describe these structures (Chopra *et al.* 1995). Adapted with permission from Chopra *et al.* (1995). Copyright © Macmillan Publishers Ltd.

devices, such as nanoscale motors (Fennimore *et al.* 2003), springs (Cumings & Zettl 2000), variable resistors (Cumings & Zettl 2004) or switches (Forró 2000).

Charlier & Michenaud (1993) first quantified this easy interlayer sliding and rotation in MWNTs using DFT calculations. Kolmogorov & Crespi (2000) introduced a new registry-dependent potential that takes into account the chiralities of interacting layers, their relative orientation and separation, and predicted that geometrically perfect MWNTs could be the ‘smoothest bearings’ (Kolmogorov & Crespi 2000), with vanishingly small interlayer friction that would not scale with the tube size in the case of incommensurate tube pairs. Such behaviour would be similar to experimentally observed ultralow friction in graphite (Dienwiebel *et al.* 2004). Other theoretical models predict friction due to interaction between the core’s end and the casing in various scenarios (Zhao *et al.* 2003; Tangney *et al.* 2004; Xia & Curtin 2004) or thermally induced fluctuations (Servantie & Gaspard 2003). Some of these models predict extensive friction, proportional to the size of the system. This wealth of somewhat contradicting theoretical models clearly demonstrates that CNTs could also be an interesting system for studying friction at the nanoscale.

First measurements of interlayer cohesive energy in MWNTs are based on TEM observations by Chopra *et al.* (1995) who discovered that in certain cases MWNTs can collapse, forming ribbons (figure 9).

This collapse is driven by a decrease in energy due to interlayer attraction that is balanced by an increase in curvature at the edges of the collapsed nanotube (figure 9b). The same authors then used an elastic model that allowed them to establish the critical radius above which tubes collapse due to van der Waals interaction between the layers and estimated that the magnitude of interlayer cohesive energy in MWNTs is 0.035 eV per atom.

The first nanomechanical experiment that highlights the easy interlayer sliding in MWNTs was carried out by Cumings & Zettl (2000) who succeeded in attaching a MWNT onto a piezoelectrically driven nanomanipulator operated

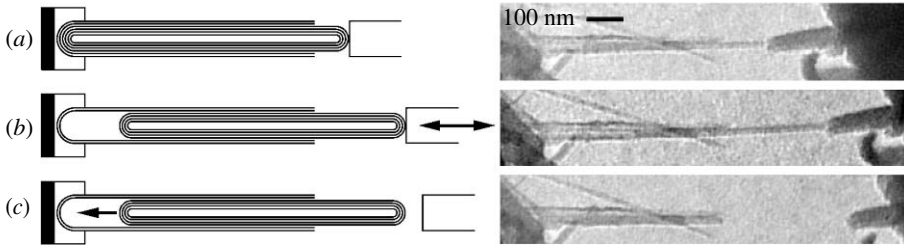


Figure 10. Schematic accompanying TEM images of the experiment performed by Cumings & Zettl (2000). (a) A carbon nanotube attached to a contact was opened at one end by applying a voltage pulse. (b) The mobile probe was attached to the protruding core and moved in the axial direction. (c) After the core had been released, it completely retracted into the tube due to van der Waals cohesion. Reprinted with permission from Cumings & Zettl (2000). Copyright © AAAS.

inside a TEM, opening the other end of the nanotube (figure 10a) and mechanically manipulating the protruding core (figure 10b). After approximately 20 cycles, no wear was observed on TEM images of the telescoping nanotube. Furthermore, after the core was released, it had fully retracted into the nanotube (figure 10c) due to the attractive interlayer van der Waals potential.

This restoring force due to interlayer van der Waals force is given by (Benedict 1998)

$$F_{\text{vdW}} = -\frac{d}{dx} U(x) = -\gamma C = -0.16C, \quad (2.8)$$

where $U(x)$ is the van der Waals potential energy; γ the interlayer cohesive energy density for a single MWNT layer; C the circumference of the ‘active’ nanotube bearing cylinder; and x the length of the overlap between the core section and the outer layer. It is interesting to note that the interlayer force is independent of the overlap length. For the nanotube in figure 10, the van der Waals force was estimated to be 9 nN. Based on the observation that complete retraction occurred between two frames of the video recording ($\Delta t = 33$ ms), Cumings & Zettl estimated limits on the static friction force $f_s < 23$ fN per atom and the dynamic friction force $f_d < 15$ fN per atom.

As these limits were based on estimates, it was however unclear at this point what the magnitude of interlayer force and friction would be, if the interlayer friction would scale with the length of the moving segment, and how it would evolve during prolonged actuation and damage to the nanotube. The magnitude of the surface energy was also based on an estimate. In order to clarify these points, Kis *et al.* performed precise force measurements on telescoping nanotubes using a TEM *in situ* manipulator with an AFM cantilever acting as a force sensor (Kis *et al.* 2006) in a geometry similar to the one shown in figure 10. Cycling telescoping motion was induced by the piezo-driven actuator while the force was measured as the deflection of the AFM cantilever. From force measurements, the interlayer cohesive energy density γ was found to be in the 0.14–0.2 J m⁻² range, corresponding to the interlayer cohesive energies between 23 and 33 meV per atom.

The measured force (figure 11a) did not show any detectable sign of periodic oscillation due to the interlayer corrugation. It was instead dominated by force fluctuations of the order of 100 pN, presumably due to stable defects like the

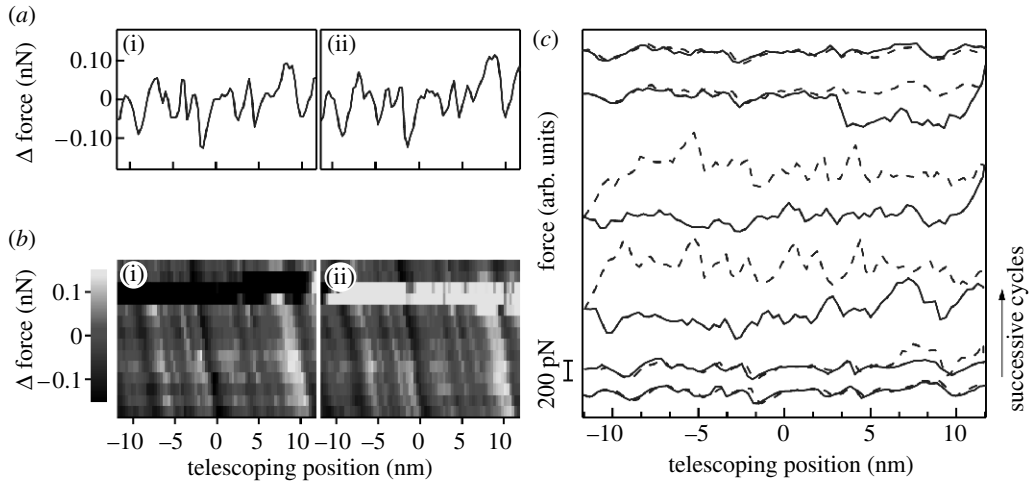


Figure 11. (a) Force acting on the telescoping core during cyclic actuation. (b) Greyscale force map for 14 cycles of motion for both telescoping directions (a(i),b(i) inward, a(ii),b(ii) outward). Dark and bright horizontal streaks indicate short-lived occurrence of mechanical dissipation. (c) A detailed plot of the last six sequential cycles of telescoping motion from (b). Solid and dashed lines represent inward and outward motions of the core with respect to the outer casing. First two cycles show virtually no hysteresis, indicating movement with no observable friction. Mechanical dissipation with irregular stick-slip-like features can spontaneously occur (curves in the middle); however, the smooth motion is rapidly restored, demonstrating the self-repairing behaviour of carbon nanotube-based linear bearings (Kis *et al.* 2006).

Stone–Wales defect (Stone & Wales 1986). The majority of observed force traces were virtually free of mechanical hysteresis, implying the absence of friction larger than 1.4 fN per atom, based on the precision of the instrumentation. Mechanical dissipation was found to spontaneously appear, manifested as streaks in the force image shown in figure 11b. Such hysteretic behaviour turns out to be short lived and generally disappears after several cycles of motion. This was attributed to the formation of reactive defects on the telescoping interface, due to electron beam irradiation followed by healing that optimizes the atomic structure and restores the original force signature (figure 11c).

Together with the ultralow friction, this self-repairing mechanism makes MWNTs even more attractive as constitutive elements in nanoelectromechanical systems (NEMS), and much more suitable for this purpose than, for example, silicon (Tanner *et al.* 2000).

3. Practical applications of CNTs in NEMS

The superior mechanical properties of CNTs, together with the prospect of realizing practically frictionless bearings prompted a very vigorous effort into realizing long-dreamt-of practical applications of CNTs as constitutive elements in NEMS, such as nanomotors, switches and high-frequency oscillators. Some of these will be reviewed in the following subsections.

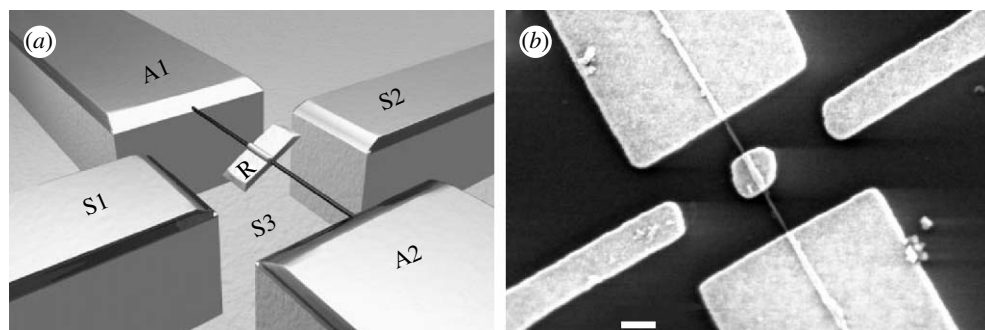


Figure 12. (a) Schematic of the nanomotor based on MWNTs realized by Fennimore *et al.* (2003). The rotor plate R is attached to a MWNT that acts as a support shaft. It is electrically contacted through A1 and A2 anchor electrodes. Stator electrodes S1, S2 and the bottom gate S3 are used to electrostatically induce rotor deflections. (b) SEM image of the MWNT-based nanomotor (Fennimore *et al.* 2003).

(a) Nanomotors

The weak van der Waals interlayer interaction in MWNTs (Charlier & Michenaud 1993) together with the rigid structure and theoretically predicted low resistance to rotational motion prompted Fennimore *et al.* (2003) to construct the first electrical motor using CNTs as the rotational element (figure 12). Their NEMS actuator was constructed using electron beam lithography starting from arc-discharge grown MWNTs deposited on an electrically conductive substrate covered with 1 μm of SiO_2 . The actuator components (figure 12b)—rotor plate (R), stator electrodes (S1 and S2) and anchor leads (A1 and A2)—were patterned using e-beam lithography followed by the deposition of Cr/Au metallic layers. HF etching was employed to remove roughly 500 nm of SiO_2 and thus suspend the whole structure, providing clearance for the rotor (R).

In order to complete the nanomotor construction, outer MWNT shells were removed in the region between rotor (R) and anchor electrodes (A1, A2). This was achieved by applying a relatively large electrical voltage (of the order of 80 V) to stator electrodes, resulting in large torsional deformation and eventual mechanical failure of outer shells. After this fabrication step, the rotor and the small MWNT segment attached to it were free to rotate on the inner shells of the MWNT axle (figure 12b). The authors were then able to drive the motor inside a scanning electron microscope for many thousands of cycles without apparent wear or decrease in performance. The authors later improved this fabrication technique by combining it with controlled deposition and microfluidic alignment of MWNTs, allowing the fabrication of arrays of aligned torsional NEMS devices based on MWNTs (Yuzvinsky 2006).

(b) Nanotube-based switches

The first nanotube-based switch demonstrated by Ruecks *et al.* (2000) was in a crossbar geometry. The device is a proof of concept for a non-volatile random access memory and consists of suspended CNTs that act as bistable switches (figure 13). Bistability in this device arises from the interplay of the elastic

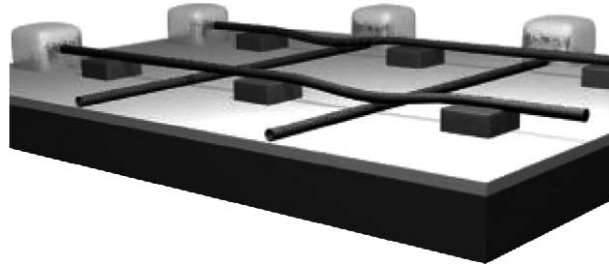


Figure 13. Conceptual drawing of the nanotube-based memory proposed by Rueckes *et al.* (2000). The device consists of an array of suspended nanotube crossbars. Reprinted with permission from Rueckes *et al.* (2000). Copyright © AAAS.

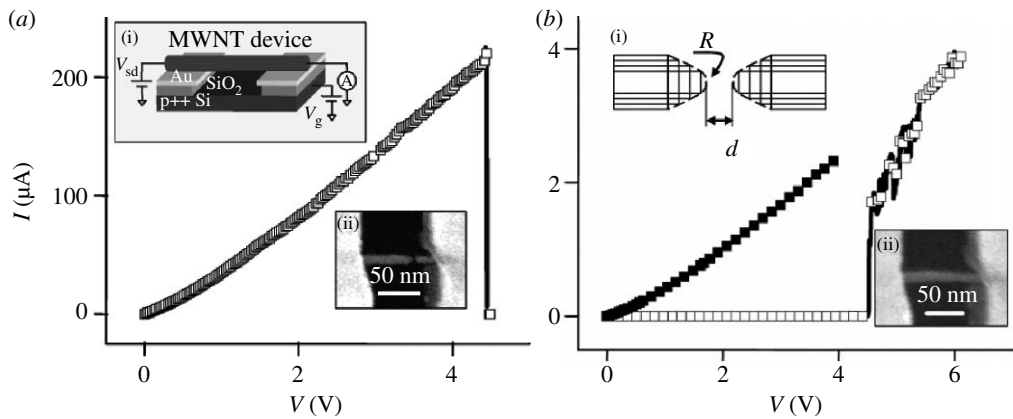


Figure 14. (a) Current–voltage characteristic of the suspended MWNT during voltage ramp leading to breakdown. The inset (i) shows the device geometry with attached electrodes and back gate. Inset (ii) is an SEM image with the gap caused by electrical breakdown. (b) Switching characteristic of the device. (i) At a sufficiently high source–drain voltage, the nanotube’s cores are electrostatically attracted thereby closing the switch. The device can be cycled by applying a sufficiently high gate voltage that causes the nanotube to bend and the cores to separate and retract. Inset (ii) shows the same device as in the inset of (a) in the closed state (Deshpande *et al.* 2006). Reprinted with permission from Deshpande *et al.* (2006). Copyright © American Chemical Society.

energy in the bent nanotube and the van der Waals attraction between tubes forming the crossbar junction. The device can be switched by applying voltages between nanotubes that result in electrostatic forces. Once in the ON state, the device can be ‘read’ using a small bias voltage and ‘reset’ using a larger voltage to produce repulsive electrostatic forces.

A commercial product based on this concept could soon be available as an alternative to flash memory.

Another interesting example of a carbon nanotube-based switch was presented by Deshpande *et al.* (2006). The operation of this switch is based on weak interlayer interaction in telescoping nanotubes (Cumings & Zettl 2000). The device consists of a MWNT suspended between source and drain electrodes. Initially the nanotube shorts these two contacts. Electrical breakdown is used to form a gap in the nanotube and open the switch (figure 14a). The switch can

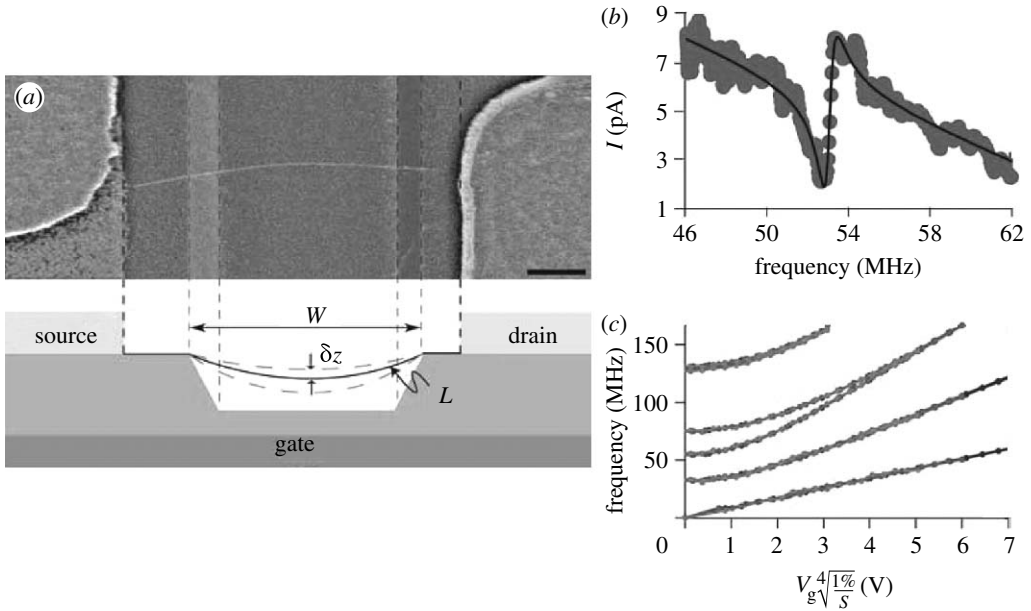


Figure 15. (a) Device geometry of the carbon nanotube oscillator developed by Sazonova *et al.* A nanotube is grown using CVD on a SiO₂ surface and suspended above a trench. The scale bar is 300 nm long. (b) Frequency response of the source–drain current through the oscillating nanotube. The solid line is a Lorentzian fit to the data yielding a resonant frequency of 55 MHz and quality factor $Q=80$. (c) Calculated predictions for the dependence of vibration frequency on gate voltage, for different amounts of slack in the suspended tube (Sazonova *et al.* 2004). Adapted with permission from Sazonova *et al.* (2004). Copyright © Macmillan Publishers Ltd.

then be closed by applying a source–drain voltage. The electrostatic force at one point causes the cores to slide out of the two nanotube segments, join in the middle through van der Waals interaction and close the electrical circuit. The switch is then cycled by applying a sufficiently high gate voltage that causes the nanotube to bend and the cores to separate and retract into the two nanotube segments.

(c) Oscillators

Owing to their low mass, nanoscale physical dimensions and Young’s modulus that can be in the TPa range, CNTs are also excellent candidates for electromechanical oscillators, with operating frequencies that could be in the GHz range. Furthermore, nanotubes can act as transistors and provide an electrical read-out of their motion. Their chemical inertness should avoid problems associated with roughness and defects, which in lithographically prepared NEMS invariably lead to high mechanical dissipation.

These exciting properties of nanotubes led several research groups to study potential applications of CNTs in NEMS oscillators. The first self-sensing nanotube oscillator was reported by Sazonova *et al.* (2004) and was based on catalytically grown CNTs suspended over trenches in SiO₂ between two metal electrodes (figure 15a).

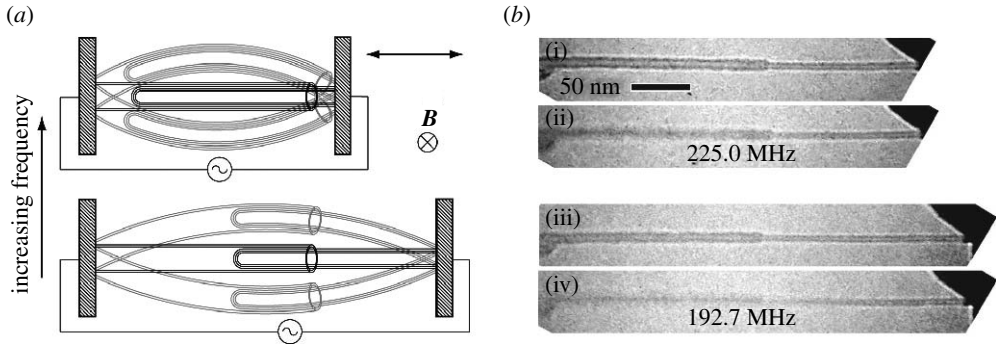


Figure 16. (a) Schematic of the tunable oscillator introduced by Jensen *et al.* A MWNT is suspended between a stationary wire and a mobile piezo-driven electrode. The device is operated in the TEM objective's magnetic field B via the Lorentz force. The resonant frequency can be tuned by varying the length of the telescoping nanotube. (b) TEM images of the oscillating nanotube off resonance (sharp, (i) and (iii)) and at resonance ((ii) and (iv); Jensen *et al.* 2006).

Nanotube oscillation is excited by applying a voltage signal at frequency ω to the gate, via electrostatic interaction with the bottom gate electrode. The nanotube is used as a mixer (Knobel & Cleland 2003) allowing the motion to be detected by simply measuring the amplitude of the source–drain current (figure 15*b*). The device can also be tuned by applying a DC voltage to the gate, which produces an electrostatic force that changes the tension in the nanotube (figure 15*c*). Sazonova *et al.* achieved resonant frequencies up to 200 MHz. Their device was however operated in vacuum and no resonance was detectable at pressures above 10 torr (1333 Pa).

This serious problem was solved by Peng *et al.* (2006) in the next generation of nanotube-based oscillators that used shorter nanotubes, with lengths of the order of 200 nm, local self-aligned gates and more importantly a new detection technique that they referred to as the ‘ 2ω ’ method. In this method, the actuation signal is applied to the gate at frequency ω , while the carrier signal is applied to the drain at $2\omega - \Delta\omega$ instead of $\omega - \Delta\omega$. This allowed the operating frequency to be pushed above the 1 GHz barrier and allowed device operation in air at 1.3 GHz, with quality factor $Q=10$, due to the much improved sensitivity of the 2ω method.

The intershell coupling was also employed by Jensen *et al.* who used the telescoping nanotube geometry (Cumings & Zettl 2000) to realize tunable MWNT oscillators (Jensen *et al.* 2006). They suspended MWNTs between a stationary electrical contact and a piezo-driven electrode in an *in situ* TEM nanomanipulator (figure 16). Oscillations were excited by applying an AC voltage to the nanotube which resulted in the Lorentz force due to the TEM objective's magnetic field. By changing the length of the telescoping nanotube, they were able to tune the resonant frequency of the nanotube oscillator up to 300 MHz with relatively high quality factors, up to 1000. Furthermore, Jensen *et al.* used this geometry to study the influence of nanotube length on dissipation and found that the dissipation ($1/Q$) is proportional to the length of the nanotube resonator.

4. Conclusion

Superior mechanical properties of CNTs were one of the main driving forces behind the effort to explore properties and practical applications of this fascinating material. Nanotubes can today be grown with very high qualities and at precisely determined locations with lengths already reaching several millimetres. As a consequence of these advances, the focus of experimental work is now slowly shifting towards exploring practical applications and device architectures that would be able to fully profit from the extremely high Young's modulus and flexibility of CNTs, most notably in the fabrication of electromechanical switches and oscillators operating at ever higher frequencies.

This work was in part supported by the Director, Office of Energy Research, Office of Basic Energy Science, Division of Materials Sciences, of the US Department of Energy under contract no. DE-AC-03-76SF00098.

References

- Avouris, P. 2002 Carbon nanotube electronics. *Chem. Phys.* **281**, 429–445. (doi:10.1016/S0301-0104(02)00376-2)
- Barber, A. H., Andrews, R., Schadler, L. S. & Wagner, H. D. 2005 On the tensile strength distribution of multiwalled carbon nanotubes. *Appl. Phys. Lett.* **87**, 203 106. (doi:10.1063/1.2130713)
- Benedict, L. X., Chopra, N. G., Cohen, M. L., Zettl, A., Louie, S. G. & Crespi, V. H. 1998 Microscopic determination of the interlayer binding energy in graphite. *Chem. Phys. Lett.* **286**, 490–496. (doi:10.1016/S0009-2614(97)01466-8)
- Blakslee, O. L., Proctor, D. G., Seldin, E. J., Spence, G. B. & Weng, T. 1970 Elastic constants of compression annealed pyrolytic graphite. *J. Appl. Phys.* **41**, 3373–3382. (doi:10.1063/1.1659428)
- Blase, X., Benedict, L. X., Shirley, E. L. & Louie, S. G. 1994 Hybridization effects and metallicity in small radius carbon nanotubes. *Phys. Rev. Lett.* **72**, 1878–1881. (doi:10.1103/PhysRevLett.72.1878)
- Charlier, J.-C. & Michenaud, J.-P. 1993 Energetics of multilayered carbon tubules. *Phys. Rev. Lett.* **70**, 1858–1861. (doi:10.1103/PhysRevLett.70.1858)
- Chico, L., Crespi, V. H., Benedict, L. X., Louie, S. G. & Cohen, M. L. 1996 Pure carbon nanoscale devices: nanotube heterojunctions. *Phys. Rev. Lett.* **76**, 971–974. (doi:10.1103/PhysRevLett.76.971)
- Chopra, N. G. & Zettl, A. 1998 Measurement of the elastic modulus of a multi-wall boron nitride nanotube. *Solid State Commun.* **105**, 297–300. (doi:10.1016/S0038-1098(97)10125-9)
- Chopra, N. G., Benedict, L. X., Crespi, V. H., Cohen, M. L., Louie, S. G. & Zettl, A. 1995 Fully collapsed carbon nanotubes. *Nature* **377**, 135. (doi:10.1038/377135a0)
- Collins, P. G., Bradley, K., Ishigami, M. & Zettl, A. 2000 Extreme oxygen sensitivity of electronic properties of carbon nanotubes. *Science* **287**, 1801–1804. (doi:10.1126/science.287.5459.1801)
- Cummings, J. & Zettl, A. 2000 Low-friction nanoscale linear bearing realized from multiwall carbon nanotubes. *Science* **289**, 602–604. (doi:10.1126/science.289.5479.602)
- Cummings, J. & Zettl, A. 2004 Localization and nonlinear resistance in telescopically extended nanotubes. *Phys. Rev. Lett.* **93**, 086801. (doi:10.1103/PhysRevLett.93.086801)
- Dai, H., Hafner, J. H., Rinzler, A. G., Colbert, D. T. & Smalley, R. E. 1996 Nanotubes as nanoprobe in scanning probe microscopy. *Nature* **384**, 147–150. (doi:10.1038/384147a0)
- de Heer, W. A., Châtelain, A. & Ugarte, D. 1995 A carbon nanotube field-emission electron source. *Science* **270**, 1179–1180. (doi:10.1126/science.270.5239.1179)

- Deshpande, V. V., Chiu, H.-Y., Postma, H. W. Ch., Mikó, C., Forró, L. & Bockrath, M. 2006 Carbon nanotube linear bearing nanoswitches. *Nano Lett.* **6**, 1092–1095. (doi:10.1021/nl052513f)
- Dienwiebel, M., Verhoeven, G. S., Pradeep, N., Frenken, J. W. M., Heimberg, J. A. & Zandbergen, H. W. 2004 Superlubricity of graphite. *Phys. Rev. Lett.* **92**, 126101. (doi:10.1103/PhysRevLett.92.126101)
- Fennimore, A. M., Yuzvinsky, T. D., Han, W. Q., Fuhrer, M. S., Cumings, J. & Zettl, A. 2003 Rotational actuators based on carbon nanotubes. *Nature* **424**, 408–410. (doi:10.1038/nature01823)
- Forró, L. 2000 Nanotechnology—beyond Gedanken experiments. *Science* **289**, 560–561. (doi:10.1126/science.289.5479.560)
- Fujii, T., Suzuki, M., Miyashita, M., Yamaguchi, M., Onuki, T., Nakamura, H., Matsubara, T., Yamada, H. & Nakayama, K. 1991 Micropattern measurement with an atomic force microscope. *J. Vac. Sci. Technol. B* **9**, 666–669. (doi:10.1116/1.585483)
- Gere, J. M. & Timoshenko, S. P. 1984 *Mechanics of materials*. Boston, MA: PWS-Kent.
- Hernández, E., Goze, C., Bernier, P. & Rubio, A. 1998 Elastic properties of C and $B_xC_yN_z$ composite nanotubes. *Phys. Rev. Lett.* **80**, 4502–4505. (doi:10.1103/PhysRevLett.80.4502)
- Iijima, S. 1991 Helical microtubules of graphitic carbon. *Nature* **354**, 56–58. (doi:10.1038/354056a0)
- Jensen, K., Girit, C., Mickelson, W. & Zettl, A. 2006 Tunable nanoresonators constructed from telescoping nanotubes. *Phys. Rev. Lett.* **96**, 215 503. (doi:10.1103/PhysRevLett.96.215503)
- Kaplan-Ashiri, I., Cohen, S. R., Gartsman, K., Ivanovskaya, V., Heine, T., Seifert, G., Wiesel, I., Wagner, H. D. & Tenne, R. 2006 On the mechanical behavior of WS_2 nanotubes under axial tension and compression. *Proc. Natl Acad. Sci. USA* **103**, 523–528. (doi:10.1073/pnas.0505640103)
- Kiang, C.-H., Endo, M., Ajayan, P. M., Dresselhaus, G. & Dresselhaus, M. S. 1998 Size effects in carbon nanotubes. *Phys. Rev. Lett.* **81**, 1869–1872. (doi:10.1103/PhysRevLett.81.1869)
- Kis, A., Csányi, G., Salvétat, J.-P., Lee, T.-N., Couteau, E., Kulik, A. J., Benoit, W., Brugger, J. & Forró, L. 2004 Reinforcement of single-walled carbon nanotube bundles by intertube bridging. *Nat. Mater.* **3**, 153–157. (doi:10.1038/nmat1076)
- Kis, A., Jensen, K., Aloni, S., Mickelson, W. & Zettl, A. 2006 Interlayer forces and ultralow sliding friction in multiwalled carbon nanotubes. *Phys. Rev. Lett.* **97**, 025501. (doi:10.1103/PhysRevLett.97.025501)
- Knobel, R. G. & Cleland, A. N. 2003 Nanometre-scale displacement sensing using a single-electron transistor. *Nature* **424**, 291–293. (doi:10.1038/nature01773)
- Kolmogorov, A. N. & Crespi, V. H. 2000 Smoothest bearings: interlayer sliding in multiwalled carbon nanotubes. *Phys. Rev. Lett.* **85**, 4727–4730. (doi:10.1103/PhysRevLett.85.4727)
- Kong, J., Soh, H. T., Cassell, A. M., Quate, C. F. & Dai, H. 1998 Synthesis of individual single-walled carbon nanotubes on patterned silicon wafers. *Nature* **395**, 878–881. (doi:10.1038/27632)
- Li, W. Z., Xie, S. S., Qian, L. X., Chang, B. H., Zou, B. S., Zhou, W. Y., Zhao, R. A. & Wang, G. 1996 Large-scale synthesis of aligned carbon nanotubes. *Science* **274**, 1701–1703. (doi:10.1126/science.274.5293.1701)
- Lu, J. P. 1997 Elastic properties of carbon nanotubes and nanoropes. *Phys. Rev. Lett.* **79**, 1297–1300. (doi:10.1103/PhysRevLett.79.1297)
- Lukić, B. *et al.* 2005a Elastic modulus of multi-walled carbon nanotubes produced by catalytic chemical vapour deposition. *App. Phys. A* **80**, 695–700. (doi:10.1007/s00339-004-3100-5)
- Lukić, B. *et al.* 2005b Catalytically grown carbon nanotubes of small diameter have a high Young's modulus. *Nano Lett.* **5**, 2074–2077. (doi:10.1021/nl051034d)
- Mintmire, J. W., Dunlap, B. I. & White, C. T. 1992 Are fullerene tubules metallic? *Phys. Rev. Lett.* **68**, 631–634. (doi:10.1103/PhysRevLett.68.631)
- Peng, H. B., Chang, C. W., Aloni, S., Yuzvinsky, T. D. & Zettle, A. 2006 Ultrahigh frequency nanotube resonators. *Phys. Rev. Lett.* **97**, 087203. (doi:10.1103/PhysRevLett.97.087203)

- Poncharal, P., Wang, Z. L., Ugarte, D. & de Heer, W. A. 1999 Electrostatic deflections and electromechanical resonances of carbon nanotubes. *Science* **283**, 1513–1516. (doi:10.1126/science.283.5407.1513)
- Rueckes, T., Kim, K., Joselevich, E., Tseng, G. Y., Cheung, C.-L. & Lieber, C. M. 2000 Carbon nanotube-based nonvolatile random access memory for molecular computing. *Science* **289**, 94–97. (doi:10.1126/science.289.5476.94)
- Saito, R., Fujita, M., Dresselhaus, G. & Dresselhaus, M. S. 1992 Electronic structure of chiral graphene tubules. *Appl. Phys. Lett.* **60**, 2204–2206. (doi:10.1063/1.107080)
- Salvetat, J.-P. *et al.* 1999a Elastic modulus of ordered and disordered multiwalled carbon nanotubes. *Adv. Mater.* **11**, 161–165. (doi:10.1002/(SICI)1521-4095(199902)11:2<161::AID-ADMA161>3.0.CO;2-J)
- Salvetat, J.-P., Bonard, J.-M., Thomson, N. H., Kulik, A. J., Forro, L., Benoit, W. & Zuppiroli, L. 1999b Mechanical properties of carbon nanotubes. *Appl. Phys. A* **69**, 255–260. (doi:10.1007/s003390050999)
- Salvetat, J.-P., Briggs, G. A. D., Bonard, J.-M., Bacsá, R. R., Kulik, A. J., Stöckli, T., Burnham, N. A. & Forró, L. 1999c Elastic and shear moduli of single-walled carbon nanotube ropes. *Phys. Rev. Lett.* **82**, 944–947. (doi:10.1103/PhysRevLett.82.944)
- Sazonova, V., Yaish, Y., Üstünel, H., Roundy, D., Arias, T. A. & McEuen, P. L. 2004 A tunable carbon nanotube electromechanical oscillator. *Nature* **431**, 284–287. (doi:10.1038/nature02905)
- Seldin, E. J. & Nezbeda, C. W. 1970 Elastic constants and electron-microscope observations of neutron-irradiated compression-annealed pyrolytic and single-crystal graphite. *J. Appl. Phys.* **41**, 3389–3400. (doi:10.1063/1.1659430)
- Servantie, J. & Gaspard, P. 2003 Methods of calculation of a friction coefficient: application to nanotubes. *Phys. Rev. Lett.* **91**, 185503. (doi:10.1103/PhysRevLett.91.185503)
- Stone, A. J. & Wales, D. J. 1986 Theoretical studies of icosahedral C₆₀ and some related species. *Chem. Phys. Lett.* **128**, 501–503. (doi:10.1016/0009-2614(86)80661-3)
- Tangney, P., Louie, S. G. & Cohen, M. L. 2004 Dynamic sliding friction between concentric carbon nanotubes. *Phys. Rev. Lett.* **93**, 065503. (doi:10.1103/PhysRevLett.93.065503)
- Tanner, D. M. *et al.* 2000 *MEMS reliability: infrastructure, test structures, experiments and failure modes*. Albuquerque, NM: Sandia National Laboratories.
- Thess, A. *et al.* 1996 Crystalline ropes of metallic carbon nanotubes. *Science* **273**, 483–487. (doi:10.1126/science.273.5274.483)
- Thostenson, E. T., Ren, Z. & Chou, T.-W. 2001 Advances in the science and technology of carbon nanotubes and their composites: a review. *Comp. Sci. Technol.* **61**, 1899–1912. (doi:10.1016/S0266-3538(01)00094-X)
- Treacy, M. M. J., Ebbesen, T. W. & Gibson, J. M. 1996 Exceptionally high Young's modulus observed for individual carbon nanotubes. *Nature* **381**, 678–680. (doi:10.1038/381678a0)
- Vigolo, B., Pénicaud, A., Coulon, C., Sauder, C., Pailler, R., Journet, C., Bernier, P. & Poulin, P. 2000 Macroscopic fibers and ribbons of oriented carbon nanotubes. *Science* **290**, 1331–1334. (doi:10.1126/science.290.5495.1331)
- Walters, D. A., Ericson, L. M., Casavant, M. J., Liu, J., Colbert, D. T., Smith, K. A. & Smalley, R. E. 1999 Elastic strain of freely suspended single-wall carbon nanotube ropes. *Appl. Phys. Lett.* **74**, 3803–3805. (doi:10.1063/1.124185)
- Wong, E. W., Sheehan, P. E. & Lieber, C. M. 1997 Nanobeam mechanics: elasticity, strength, and toughness of nanorods and nanotubes. *Science* **277**, 1971–1975. (doi:10.1126/science.277.5334.1971)
- Xia, Z. & Curtin, W. A. 2004 Pullout forces and friction in multiwall carbon nanotubes. *Phys. Rev. B* **69**, 233408. (doi:10.1103/PhysRevB.69.233408)
- Yakobson, B. I., Brabec, C. J. & Bernholc, J. 1996 Nanomechanics of carbon tubes: instabilities beyond linear range. *Phys. Rev. Lett.* **76**, 2511–2514. (doi:10.1103/PhysRevLett.76.2511)
- Yu, M.-F., Lourie, O., Dyer, M. J., Moloni, K., Kelly, T. F. & Ruoff, R. S. 2000a Strength and breaking mechanism of multiwalled carbon nanotubes under tensile load. *Science* **287**, 637–640. (doi:10.1126/science.287.5453.637)

- Yu, M.-F., Files, B. S., Arepalli, S. & Ruoff, R. S. 2000*b* Tensile loading of ropes of single wall carbon nanotubes and their mechanical properties. *Phys. Rev. Lett.* **84**, 5552–5555. (doi:10.1103/PhysRevLett.84.5552)
- Yuzvinsky, T. D., Fennimore, A. M., Kis, A. & Zettl, A. 2006 Controlled placement of highly aligned carbon nanotubes for the manufacture of arrays of nanoscale torsional actuators. *Nanotechnology* **17**, 434–438. (doi:10.1088/0957-4484/17/2/015)
- Zhao, Y., Ma, C.-C., Chen, G. H. & Jiang, Q. 2003 Energy dissipation mechanisms in carbon nanotube oscillators. *Phys. Rev. Lett.* **91**, 175504. (doi:10.1103/PhysRevLett.91.175504)
- Zhu, H. W., Xu, C. L., Wu, D. H., Wei, B. Q., Vajtai, R. & Ajayan, P. M. 2002 Direct synthesis of long single-walled carbon nanotube strands. *Science* **296**, 884–886. (doi:10.1126/science.1066996)